


## Article

# RF-ICP Thermal Plasma for Thermoplastic Waste Pyrolysis Process with High Conversion Yield and Tar Elimination

Mohamed Aboughaly , Hossam A. Gabbar \*, Vahid Damideh and Isaac Hassen

Faculty of Energy Systems and Nuclear Science, University of Ontario Institute of Technology,  
Oshawa, ON L1G0C5, Canada; mohamed.aboughaly@uoit.net (M.A.); v\_damideh@yahoo.com (V.D.);  
isaac.hassen@ontariotechu.net (I.H.)

\* Correspondence: hossam.gabbar@uoit.ca

Received: 29 January 2020; Accepted: 26 February 2020; Published: 28 February 2020



**Abstract:** This paper demonstrates an RF thermal plasma pyrolysis reaction apparatus that achieves 89 wt.% reaction conversion yield with no tar content. The demonstrated experimental apparatus consists of a 1100 W RFVII Inc. (104 Church St, Newfield, NJ 08344, United States) @ 13.56 MHz RF thermal plasma generator, a Navio matching network, intelligent feedback controller, and an 8-turn copper RF-ICP torch embedded in a 12 L thermochemical reactor. The intelligent feedback controller optimizes the thermal performance based on feedback signals from three online gas analyzers: CO, CO<sub>2</sub> and NO<sub>x</sub>. The feedback controller output signal controls the RF thermal plasma torch current that provides real-time temperature control. The proposed reaction system achieves precise temperature profiles for both pyrolysis and gasification as well as increases end-product yield and eliminates undesired products such as tar and char. The identified hydrocarbon liquid mixture is 90 wt.% gasoline and 10 wt.% diesel. The 8-turn RF-ICP thermal plasma torch has an average heating rate of +35 °C/min and a maximum operating temperature of 2000 °C and is able to sustain stable flame for more than 30 min. The reaction operating parameters are (550–990 °C  $\tau$  = 30 min for pyrolysis and (1300 °C  $\tau$  = 1 sec) for the gasification process. The identified hydrocarbon liquid products are 90 wt.% of a n-butyl-benzene (C<sub>6</sub>H<sub>5</sub>C<sub>4</sub>H<sub>9</sub>) and oluene (C<sub>7</sub>H<sub>8</sub>) mixture with less than 10 wt.% decane diesel fuel (C<sub>10</sub>H<sub>22</sub>). Comsol simulation is used to assess the RF-ICP thermal plasma torch's thermal performance.

**Keywords:** radio frequency thermal plasma; intelligent feedback control system; process control algorithms; waste-to-energy; thermochemical processes; gasoline and diesel production; sustainable energy; time-dependent 3D comsol simulation

## 1. Introduction

Currently, global municipal solid waste (MSW) generation exceeds 2.01 billion tons per annum while untreated global solid waste depositions are expected to reach 27 billion tons by 2050 [1,2]. In Canada, non-hazardous annual solid waste generation is estimated at 25 million metric tons per annum and is considered a main source of greenhouse gas emissions in the waste management sector [3,4]. Greenhouse gaseous emissions from solid waste are released through landfilling, incineration and other uncontrolled waste management practices [5].

Plastic waste deposits are expected to form 10 to 15 wt.% of collected solid waste according to the national greenhouse gas inventory [6]. The non-residential sectors, including industrial areas, contribute to 60 wt.% of collected solid waste deposits, while the rest are from residential and diverted areas [7]. In recent years, public and political awareness has been raised to find a sustainable eco-friendly solution

for solid waste deposits with negligible greenhouse gas emissions. On the other hand, incineration and landfilling are still considered the main practices of solid waste recycling in Canada. Currently, there are only seven municipal incineration sites in Canada processing 763,000 tons/annum of MSW using conventional thermal methods such as furnaces and fired gas heaters [8,9]. The unsorted solid waste higher heating value (HHV) for thermochemical reactors is in the range of 7–10 MJ/kg while plastic waste feedstock has an HHV of 40 MJ/kg [8,10]. Below, current solid waste generation statistics in the Organization for Economic Co-operation and Development (OECD) countries are shown in Figure 1:

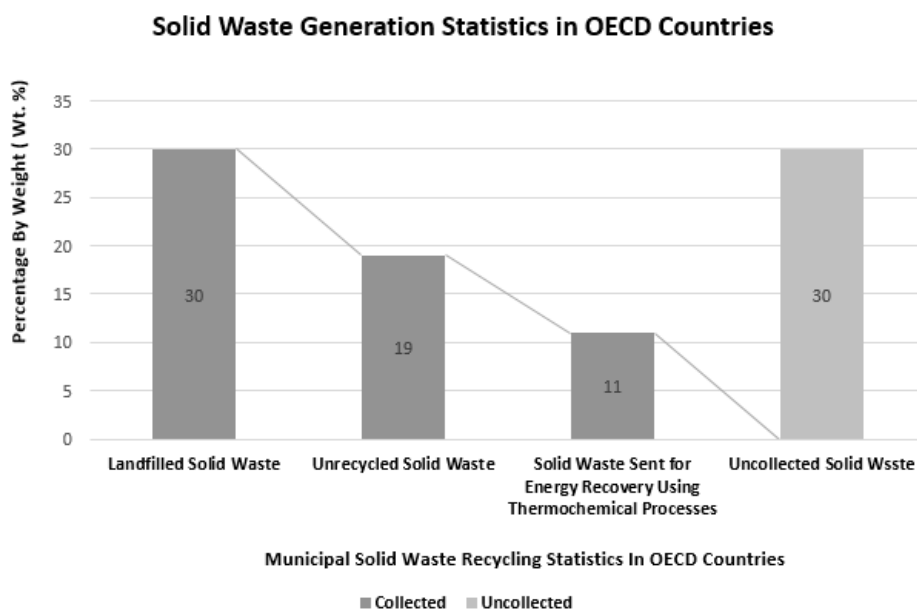


**Figure 1.** Current municipal solid waste recycling practices in the Organization for Economic Co-operation and Development (OECD) countries [1].

### 1.1. Thermochemical Processes Net Energy Production

The solid waste chemical composition and energy content varies from one feedstock to another depending on the socio-economic conditions and chemical composition in different geographical areas. The allowable elemental composition, moisture and dry ash content should be considered in the design basis of industrial gasifiers [11]. The highest energy content is produced from plasma arc gasification, combined pyrolysis and gasification, and conventional gasification, respectively, as shown in Figure 2:

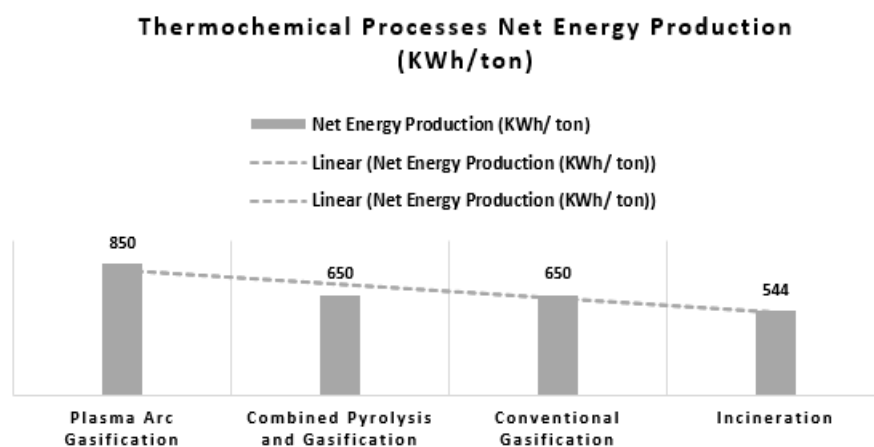


**Figure 2.** Net energy production to grid from different thermochemical processes (KWh/ton of MSW).

### 1.2. Characterization of Thermal Plasma Jets

Thermal plasma technology is a novel high thermal technique that is used in metallurgical applications such as coatings, destruction of hazardous waste as well as solid waste thermochemical reactions: incineration (I), pyrolysis (P), gasification (G) and combined pyrolysis–gasification (P-G) [12,13]. Currently, DC and AC thermal plasma jets are more commonly used, due to low cost and higher thermal efficiency. In terms of thermal efficiency, DC plasma achieves 90% while RF plasma achieves up to 75% [14]. For RF thermal plasma, the electron temperature ( $T_e$ ) is higher for CCP (Capacitively Coupled Plasma) in comparison to ICP (Inductively Coupled Plasma), while the electron density for ICP plasma is higher [12]. RF-ICP thermal plasma is recommended for thermochemical reactions. The thermal plasma characteristics are shown in Figure 3 and Table 1:

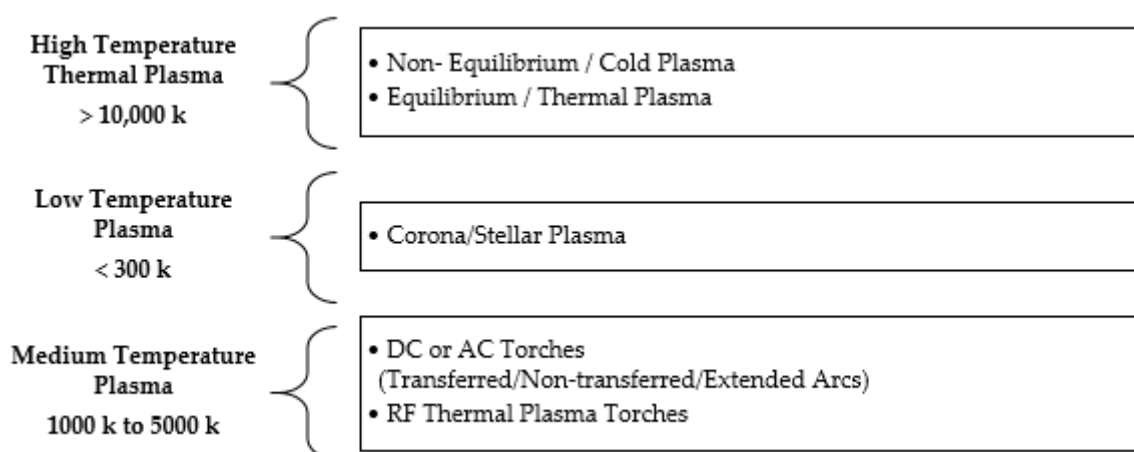


Figure 3. Categories of thermal plasma temperature characteristics.

Table 1. Operating temperatures and applications of thermal plasma jets.

Process Variable	Non-Thermal Plasma	Low Temperature Thermal Plasma	High Temperature Thermal Plasma
Operating Temperature	$T_i \approx T_e < 300$ K	$T_i \approx T_e < 10^3$ K	$T_i \approx T_e > 10^6$ K
Applications	Thermal arc emissions, low pressure glow discharges	Waste-to-energy, metallurgical applications	Fusion experimental work

By definition, thermal plasma jets consist of free ions at local thermodynamic equilibrium (LTE) with small spatial variations giving high density arc discharge emissions [15]. The major advantages of RF thermal plasma jets are as follows [12]:

- High energy density ( $10^5$  W/cm<sup>2</sup>– $10^7$  W/cm<sup>2</sup>) and a high heat transfer surface area;
- A controllable reactive zone (flame) that achieves higher thermal control over reactivity;
- The presence of free ions and excited molecules that fastens reaction rates;
- Flexibility in carrier gases, either nitrogen, argon or oxygen, at low flow rates;
- High operating temperatures (1000 K to 10,000 K);
- High ionized particle concentration ( $10^{16}$ – $10^{17}$  particles/cm<sup>3</sup>).

### 1.3. Tar Tolerance Levels in Pyrolysis Reactors

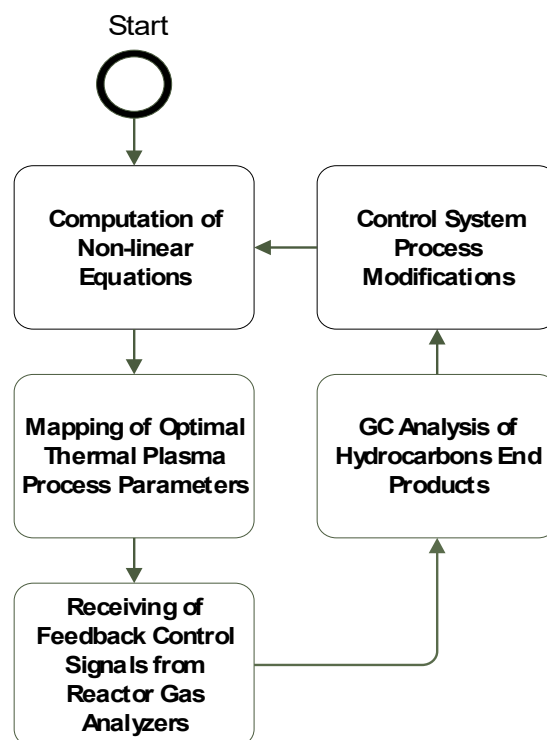
The existence of tar particles in hydrocarbon end products such as syngas and hydrocarbon liquids is a common operational problem that lowers the quality of end products and reduces the overall reaction conversion yield as well as causing severe problems and maloperations in combustion engines and gas turbines [8]. Below, the maximum allowable tar concentration levels are shown in Table 2:

**Table 2.** Maximum allowable tar rates in industrial gasification systems (g/Nm<sup>3</sup>).

Reactor Configuration	Tar Rates (g/Nm <sup>3</sup> ) Process Units			Tar Rates (g/Nm <sup>3</sup> ) Internal Combustion Engines and Turbines		
	Min	Max	Average	Min	Max	Average
<b>Updraft</b>	1	150	20–100	0.1	3	0.1–1
<b>Downdraft</b>	0.05	6	0.1–1.5	0.01	10	0.1–0.2

#### 1.4. Proposed Solution Approach

The proposed solution approach of RF thermal plasma design and integration in thermochemical reactors is shown in Figure 4 [16]:

**Figure 4.** Integration of RF thermal plasma torch in pyrolysis reaction chamber flowchart.

## 2. DC and RF Thermal Plasma Generation Systems

Thermal plasma is used in various industries such as metallurgical, welding, chemical synthesis, ceramic powder synthesis, spray coatings and thermal treatment of solid and nuclear waste deposits [17]. The behavior of thermal plasma jets is studied using static models that are able to predict thermal plasma temperature, jet velocity and electromagnetic field distributions for thermal plasma steady state configurations [18]. In these models, the non-linear temperature and velocity equations of the ionized gases and the electromagnetic fields are calculated. The conservation equations are two-dimensional (r, z) time-dependent equations that represent the dynamic torch behavior during ignition and transient conditions of the RF torch, as shown in Equation (1) to Equation (4):

$$\frac{\partial}{\partial z}(\rho u) + \frac{1}{r} \frac{\partial}{\partial r}(r \rho v) = 0 \quad (1)$$

where  $\rho$  and  $u$  are the plasma density (kg/m<sup>3</sup>) and plasma viscosity respectively.

The conservation equations of momentum include the  $z$ ,  $r$ ,  $y$  and  $\theta$  components, consider Lorentz force, and assume laminar flux and axial symmetry. The plasma momentum equations are shown below:

$$\rho\mu\frac{\partial v}{\partial z} + \rho v\frac{\partial v}{\partial r} - \eta\frac{\partial^2 v}{\partial z^2} - \frac{\eta}{r}\frac{\partial v}{\partial r} + \frac{\eta v}{r^2} - \eta\frac{\partial v}{\partial r} - \rho\omega^2 - J_e B_z = 0 \quad (2)$$

$$-\frac{\rho\mu v}{r} + \rho\mu\frac{\partial v}{\partial r} + \rho v\frac{\partial \mu}{\partial r} - \eta\frac{\partial^2 \mu}{\partial z^2} - \frac{\eta}{r}\frac{\partial \mu}{\partial r} - \eta\frac{\partial^2 \mu}{\partial r^2} + J_e B_r = 0 \quad (3)$$

$$\rho\mu\frac{\partial \omega}{\partial z} + \frac{\rho v \omega}{r} + \rho v\frac{\partial \omega}{\partial r} - \eta\frac{\partial^2 \omega}{\partial z^2} - \eta\frac{\partial \omega}{\partial r} - \eta\frac{\partial^2 \omega}{\partial r^2} + \frac{\omega \eta}{r^2} - J_r B_z = 0. \quad (4)$$

### 2.1. DC Transferred and Non-Transferred Arcs

In transferred arc reactors, one electrode is electrically conductive and is located outside the reaction chamber, while in non-transferred DC arcs, the electrodes are placed inside the reactor. The electrodes of non-transferred DC torches are usually larger in size and have higher wear and tear.

### 2.2. RF Inductively Coupled (ICP) and Capacitively Coupled (CCP) Thermal Plasma

Inductively coupled thermal plasma (ICP) is a more common generation method due to its higher energy density than capacitively coupled thermal plasma (CCP). For CCP plasma generation, the plasma density of the capacitively coupled torch is linear to the generation power. CCP plasma generation is lower than that of inductively thermal plasma (ICP) due to ionic energy loss [19]. In CCP plasma, the discharge current is controlled by the electrode at the plasma boundary, while in ICP, the RF current generates plasma in a closed loop without the RF sheath. The electron temperature ( $T_e$ ) is defined by the ionization balance, while the plasma density is defined by power absorbed by electrons,  $N_p = P_d$ . The main advantages of RF-ICP thermal plasma in thermochemical reactors are as follows [16]:

- Independent control of ion flux and energy density;
- Ability to operate in a wide range of frequencies and control temperature using current;
- Ability to operate at a low power and low plasma density;
- Ability to control the operating temperature using current, achieving a faster control response.

### 2.3. RF Thermal Plasma Conservation Equations and Process Control Algorithms

Flowing gas density continuity equation,  $\rho$  [20]:

$$-\frac{\partial \rho}{\partial t} + \frac{1}{r}\frac{\partial}{\partial r}(r\rho v_r) + \frac{\partial}{\partial z}(\rho v_z) = 0. \quad (5)$$

Navier–Stokes equation for the radial component of the velocity,  $v_r$  [20]:

$$\rho\left(\frac{\partial v_r}{\partial t} + v_r\frac{\partial v_r}{\partial r} + v_z\frac{\partial v_r}{\partial z}\right) = -\frac{\partial \rho}{\partial r} - 2\frac{\partial \mu v_r}{r^2} + \frac{2}{r}\frac{\partial}{\partial r}\left(\mu r\frac{\partial v_r}{\partial r}\right) + \frac{\partial}{\partial z}\left(\mu\left(\frac{\partial v_r}{\partial z} + \frac{\partial v_z}{\partial r}\right)\right) + Fr. \quad (6)$$

Navier–Stokes equation for the axial component of the velocity,  $v_z$  [20]:

$$\rho\left(\frac{\partial v_z}{\partial t} + v_r\frac{\partial v_z}{\partial r} + v_z\frac{\partial v_z}{\partial z}\right) = -\frac{\partial \rho}{\partial z} + 2\frac{\partial}{\partial z}\left(\mu\frac{\partial v_z}{\partial z}\right) + \frac{1}{r}\frac{\partial}{\partial r}\left(r\mu\left(\frac{\partial v_z}{\partial r} + \frac{\partial v_r}{\partial z}\right)\right) + Fr. \quad (7)$$

The real-time monitoring control system for the waste-to-energy thermochemical process is shown below in Figure 5:

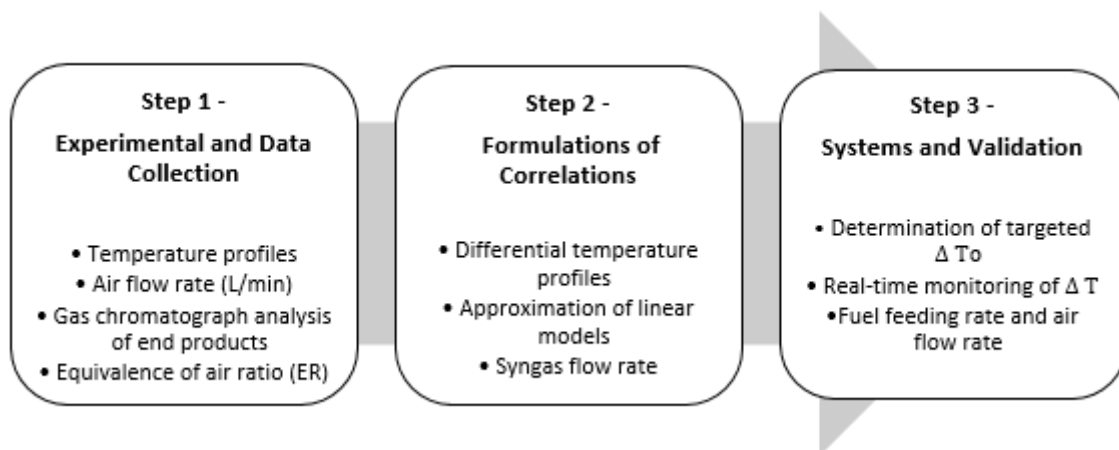


**Figure 5.** Process flow diagram for real-time monitoring control for thermochemical reactors.

#### 2.4. Process Control Modelling

##### End-Product Gas Yield Control Algorithms

The gaseous products produced during the gasification process indicate the reaction conversion efficiency.  $\eta_{\text{Gas}}$  is the ratio between the volumetric flow rate of outlet gases from the gasifier to the initial mass flow rate of the solid waste presented by the equation below [21]:

$$\eta_{\text{Gas}} = \frac{Q_{\text{Syngas}}}{M_{\text{MSW}}} \quad (8)$$

where  $Q_{\text{Syngas}}$  and  $M_{\text{MSW}}$  are the volumetric flow rate and mass flow rate of syngas and solid waste, respectively [22].

### 3. RF Thermal Plasma Simulation

The following RF-ICP simulation model demonstrates the thermal performance of the ICP thermal plasma torch in thermochemical reactions. The following assumptions are assumed in the simulation [3]:

- Thermal plasma is under a local partial thermodynamic equilibrium (LTE);
- Plasma is considered a conductive fluid mixture and is modelled using magnetohydrodynamics (MHD) equations;
- The thermal plasma jet is axisymmetric, optically thin, and at a local thermodynamic equilibrium;
- The gaseous velocity is constant at laminar flow with no tangential components;
- The displacement current and electrostatic fields are neglected.

#### 3.1. RF Torch Assumptions

- The RF thermal plasma torch model has an axisymmetric configuration;
- The torch consists of eight turns with a cross-sectional coil diameter of 3 mm;
- Flow is assumed to be steady state, laminar flow of pure argon flow at 7.5 L/min;
- The thermal plasma jet is thin and at local thermodynamic equilibrium (LTE) conditions;
- Viscous dissipation and change in pressure are neglected in energy conservation equations.

#### 3.2. RF Thermal Plasma Comsol Simulation

The Comsol model geometry for a 1000 W RF plasma torch at 13.56 MHz and argon gas flow at 7.5 L/min in the sheath tube is shown below in Figures 6–9.

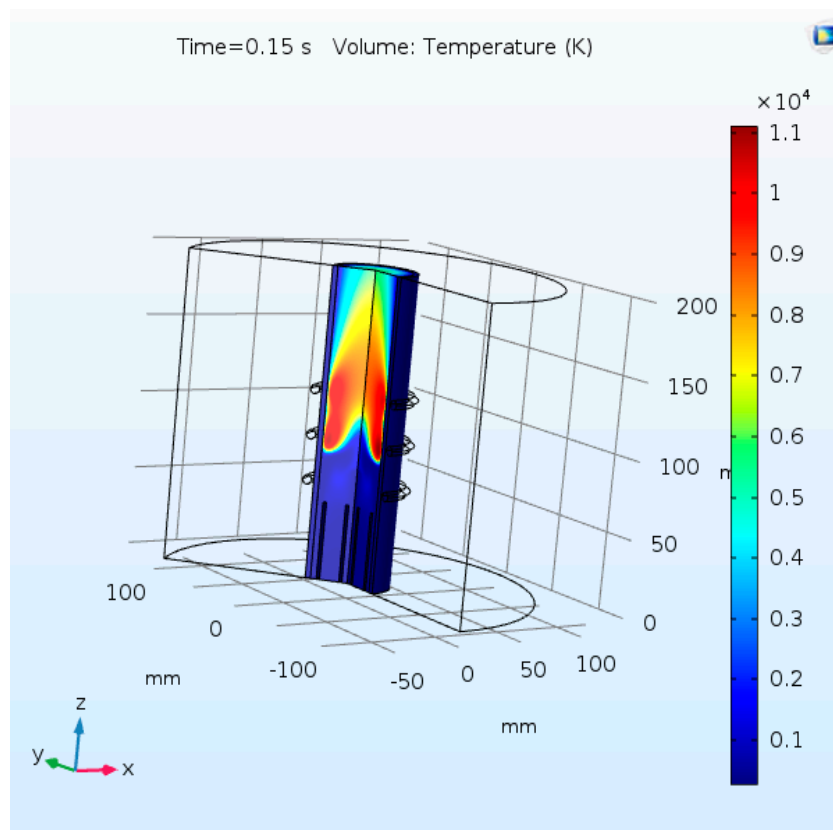


Figure 6. RF thermal plasma torch temperature profile.

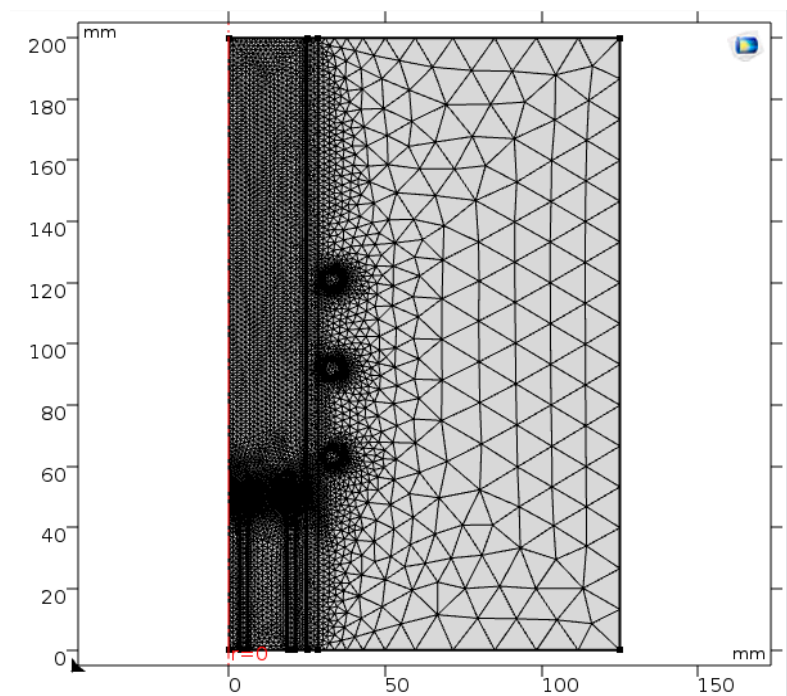


Figure 7. Meshing of the RF thermal plasma torch.

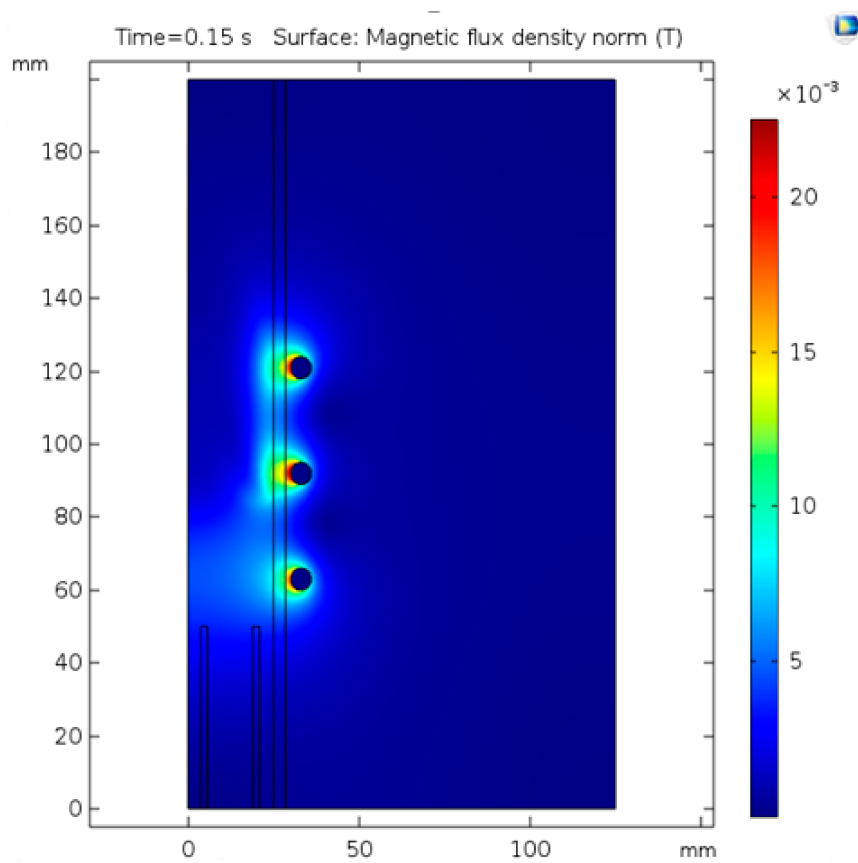


Figure 8. RF thermal plasma torch conductivity (S/m).

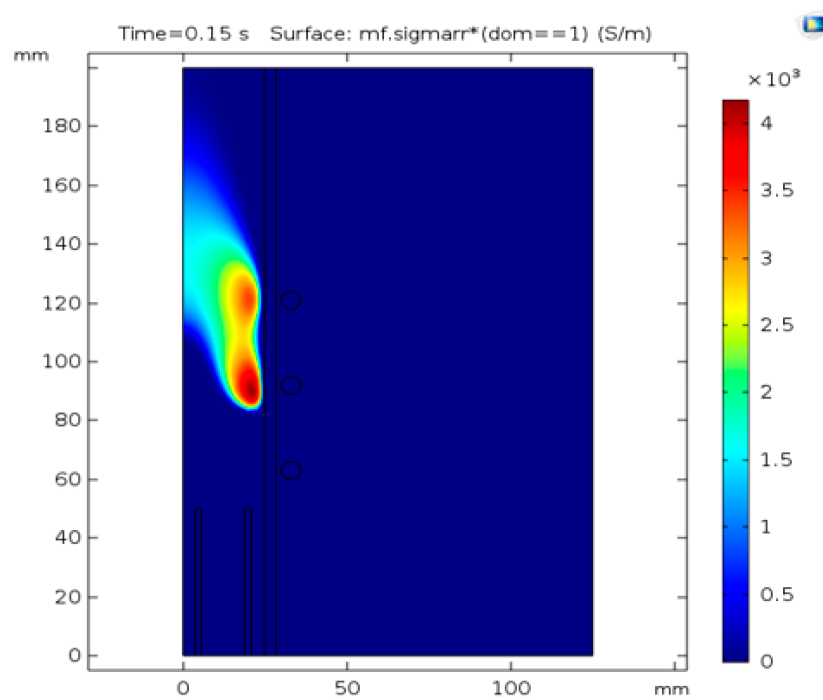


Figure 9. Surface magnetic flux density (S/m).



## 4. Experimental Apparatus

### 4.1. Equipment Description and Experimental Procedures

Shredded plastic waste is added to the closed system reactor via a side ball valve followed by continuous nitrogen gas flow and purging inside the reaction chamber. The gas analyzers give real-time gaseous measurement of the weight content (wt.%) inside the reactor for oxygen ( $O_2$ ), carbon monoxide (CO), nitrogen oxides ( $NO_x$ ) and carbon monoxide ( $CO_2$ ). The gas analyzers ensure that there is negligible oxygen content inside the reaction chamber during startup and operation. The RF thermal plasma torch is used as a primary heat source for thermochemical reactions, and the k-type thermocouple provides real-time measurement. The RF torch is used as a primary heat and thermal control source. The torch current is increased until the desired operating temperature is reached (i.e., 550 °C for Pyrolysis and 900 °C for gasification). The RF thermal plasma torch temperature is maintained during the reaction residence time until desired hydrocarbon products are produced. (For pyrolysis  $\tau = 30$  min, gasification  $\tau = 1$  sec). For pyrolysis, after completion of the reaction residence time, the thermal plasma torch is switched off and the hydrocarbon gaseous products pass through a condensation system where hydrocarbon products are condensed at room temperature and collected. The condensation system is used to condense hydrocarbon gaseous products leaving the reactor. For gasification, a continuous flow of syngas passes through a syngas turbine and then combusted for steam and electricity generation purposes. Gas samples are collected during and after experimental trials and identified using the gas chromatograph-flame ionization detector method. The GC-FID (gas chromatograph-flame ionization detector method) is used to provide molecular weight readings and identify the molecular weights of hydrocarbon gaseous and liquid end-products.

### 4.2. Equipment Setup

The RF thermal plasma reaction experimental apparatus consists of the following equipment, as shown in Figure 10:

- An RF thermal plasma cathode cooling water to prevent resistive heat;
- A constant argon gas supply at 7.5 L/min;
- Three gas analyzers: CO,  $CO_2$  and  $NO_x$ ;
- A startup graphite electrode (diameter: 10 mm);
- A 1000 W RF thermal plasma system;
- Diagnostic equipment including a gas chromatograph;
- A high-pressure steam boiler and steam turbine for energy generation.

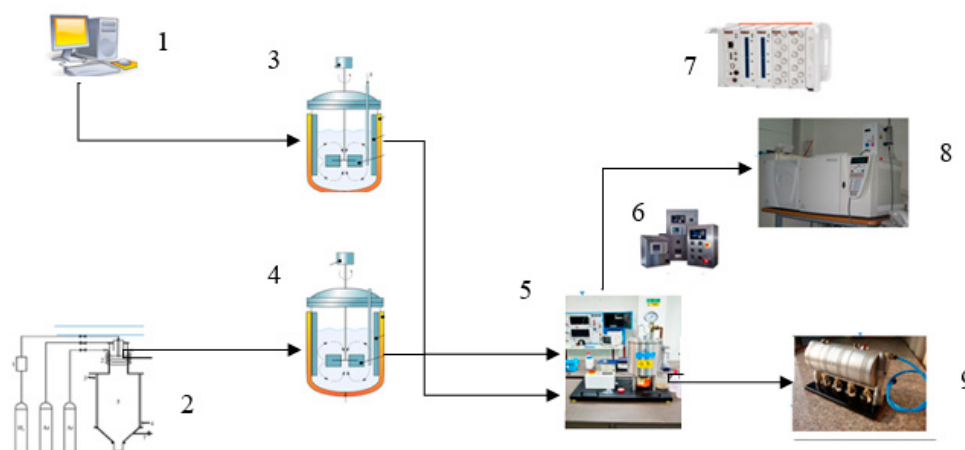


**Figure 10.** RF thermal plasma thermochemical reaction apparatus.

### Reaction Apparatus Legend

- (1). Comsol Simulation Software
- (2). Nitrogen and Argon Gas Cylinders
- (3). Pyrolysis Reactor
- (4). Gasification Reactor
- (5). Steam Boiler
- (6). Steam Turbine
- (7). DAQ (Data Acquisition System)
- (8). Gas Chromatography
- (9). Steam Turbine

### 4.3. RF Thermal Plasma Torch Dimensions and Temperature Profile

The RF Plasma torch was successfully switched on and reached a maximum operating temperature of 2000 °C. The RF torch fused quartz tube dimensions are 14 cm length, 2.5 cm outer diameter and 2.5 mm thickness. For its RF torch, a 4.7 cm length, 8 turn copper coil made by a 3 mm diameter copper tube was used. RF coil inductance was calculated to be 1.5 uH. During experimental work, the RF plasma torch was ignited using a graphite rod at constant argon gas flow at 7.5 l/min and  $\Delta$  35 °C/min. The temperature recordings are shown in Figures 11 and 12.

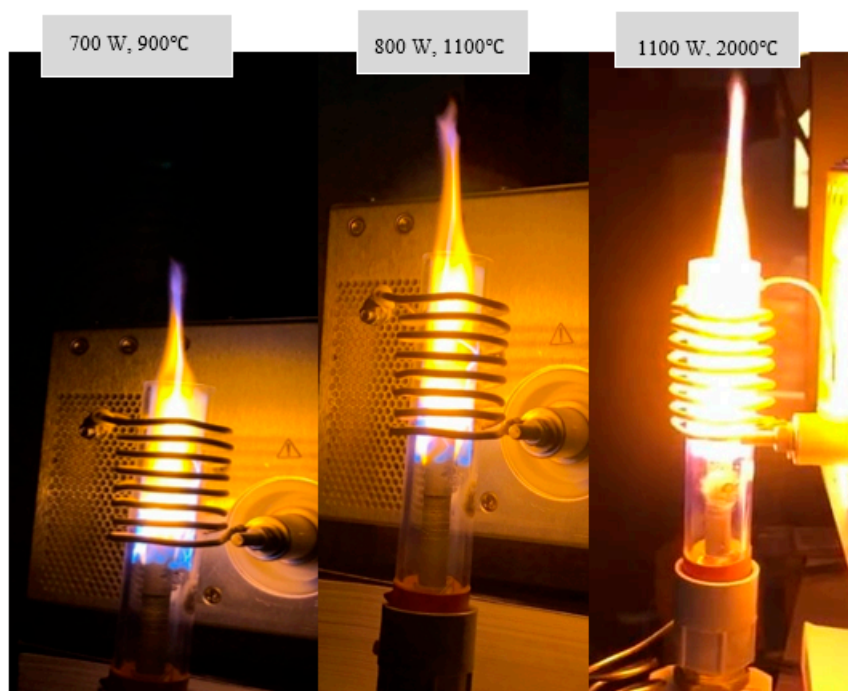


**Figure 11.** Self-ignited RF thermal plasma torch at 7.5 L/min flow exceeding 2000 °C.

### 4.4. Experimental Analysis and Results

Figure 13 shows the RF plasma torch in operation at an average heating rate of  $\Delta$  35 °C/min. Resistive heat is prevented using cooling water flow inside the hollow copper tube. The oil collected from 1 kg of thermoplastic waste mixture showed a conversion efficiency yield of 89 wt.%. The collected oil was identified using GC-FID (gas chromatograph-flame ionization detector method) showing 90 wt.% n-butyl-benzene ( $C_6H_5C_4H_9$ ) and toluene ( $C_7H_8$ ) with less than 10 wt.% decane diesel fuel ( $C_{10}H_{22}$ ). Figure 13 shows identified n-butyl-benzene ( $C_6H_5C_4H_9$ ) and toluene ( $C_7H_8$ ) as well as decane ( $C_{10}H_{22}$ ).

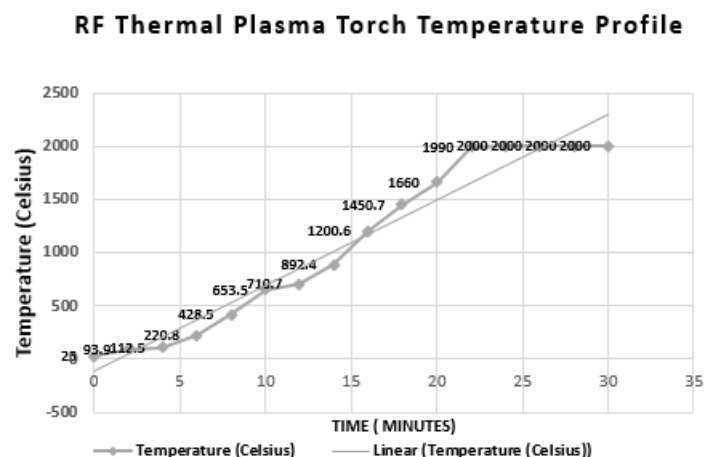


Figure 12. RF thermal plasma torch temperature reading.

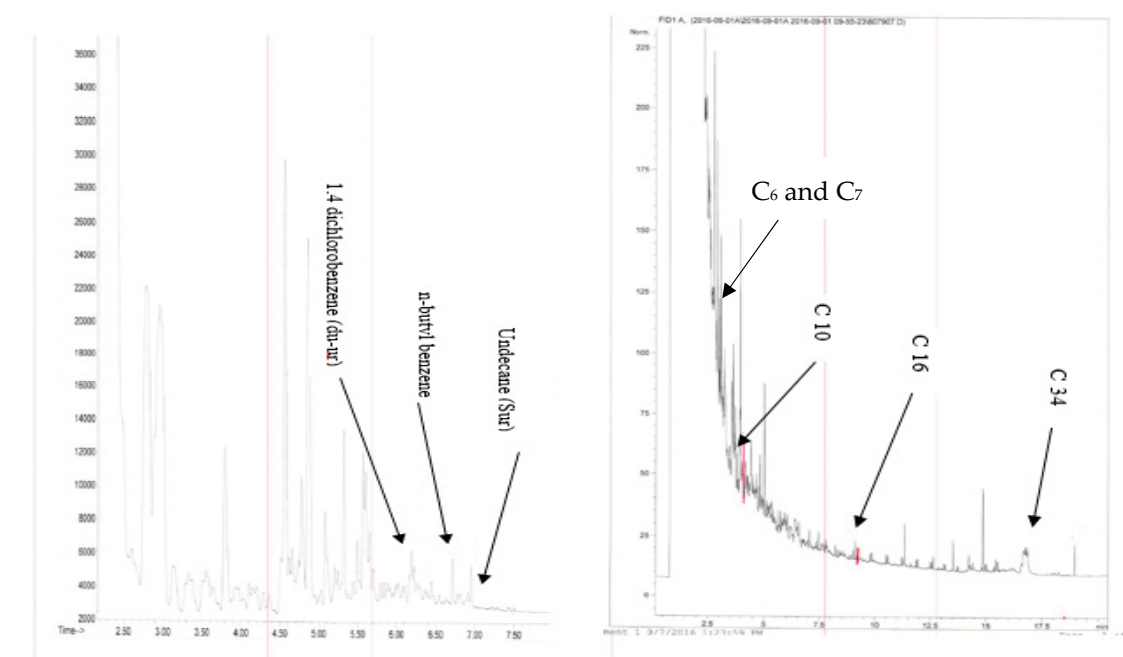


Figure 13. RF thermal plasma pyrolysis GC analysis results.

## 5. Conclusions

In conclusion, the experiment showed that an RF thermal plasma nearly eliminates the tar content which was reflected in the gas chromatograph results (i.e., C 34) as shown in Figure 13. Also, RF thermal plasma showed enhancement of the chemical reactivity of thermoplastic pyrolysis reactions. In the demonstrated experimental work, the achieved conversion efficiency was 89 wt.% for the pyrolysis process at the operating temperature (550–900 °C and above 90 wt.% for the gasification process. The RF thermal plasma torch average heating rate was +35 °C/min and reached a maximum operating temperature of 2000 °C, maintaining sustainable thermal plasma for more than 30 minutes. The collected hydrocarbon end-products were 90 wt.% n-butyl-benzene ( $C_6H_5C_4H_9$ ) and toluene ( $C_7H_8$ ) with less than 10 wt.% decane diesel fuel ( $C_{10}H_{22}$ ). Negligible tar and char were collected as residue.

**Author Contributions:** H.A.G., V.D. and M.A. carried the conceptual design and designed the experimental apparatus. V.D., M.A. and I.H. carried the experimental trials and analyzed data, M.A. wrote the paper. All authors have read and agreed to the published version of the manuscript.

**Funding:** This research was funded by Proflange Ltd., a leading Canadian stainless manufacturing company for industrial applications.

**Acknowledgments:** The thermal plasma team would like to acknowledge Proflange Ltd. for their funding and continuous support.

**Conflicts of Interest:** The authors declare no conflict of interest.

## Abbreviations & Nomenclature

### Abbreviations

CCP	Capacitively Coupled Plasma
DC	Direct Current
FID	Flame Ionization Detector Gas Chromatograph
F-T	Fischer-Tropsch process
G	Gasification
GC-FID	Gas Chromatograph-Flame Ionization Detector method
GHG	Greenhouse Gas Emissions
I	Incineration
ICP	Inductively Coupled Plasma
LDPE	Low Density Polyethylene
MSW	Municipal Solid Waste
OECD	Organization for Economic Co-operation and Development
P	Pyrolysis
P-G	Combined Pyrolysis and Gasification Process
RF	Radio Frequency

### Nomenclature

$F_r$	Force in the radial direction
$F_z$	Force in the axial direction
$F(u)$	Number of particles per $m^3$
$J_r$	Plasma flux density in radial direction, $(kg/m^3)$
K	Kelvin
KWh	kilowatt-hour
$\rho$	Density $(kg/m^3)$
$T_e$	Electron temperature, K
$T_i$	Initial operating temperature, K
$T_0$	Atmospheric temperature, K
$\partial t$	Change in time, seconds
$\tau$	Reaction residence time (minutes)
v	Velocity, (m/s)
$v_r$	Velocity in the radial direction, (m/s)
$v_z$	Velocity in the axial direction, (m/s)
wt. %	Weight percentage
$\omega^2$	Angular velocity, (m/s)
$\partial z$	Change in axial direction, m

## References

1. Kawai, K.; Tasaki, T. Revisiting estimates of municipal solid waste generation per capita and their reliability. *J. Mater. Cycles Waste Manag.* **2016**, *18*, 1–13. [[CrossRef](#)]
2. Karak, T.; Bhagat, R.M.; Bhattacharyya, P. Municipal solid waste generation, composition, and management: The world scenario. *Crit. Rev. Env. Sci. Technol.* **2012**, *42*, 1509–1630. [[CrossRef](#)]
3. Alhumid, H.A.; Haider, H.; Alsaleem, S.S.; Alinizzi, M.; Shafiqzaman, M.; Sadiq, R. Performance assessment model for municipal solid waste management systems: Development and implementation. *Environments* **2019**, *6*, 19. [[CrossRef](#)]

4. David, A. Technical Document on Municipal Solid Waste Organics Processing. Available online: [https://www.ec.gc.ca/gdd-mw/3E8CF6C7-F214-4BA2-A1A3-163978EE9D6E/13-047-ID-458-PDF\\_accessible\\_ANG\\_R2-reduced%20size.pdf](https://www.ec.gc.ca/gdd-mw/3E8CF6C7-F214-4BA2-A1A3-163978EE9D6E/13-047-ID-458-PDF_accessible_ANG_R2-reduced%20size.pdf) (accessed on 30 January 2020).
5. Niessen, W.R. Combustion and Incineration Processes. *J. Chem. Inf. Model.* **2010**, *52*, 11.
6. Mohareb, A.K.; Warith, M.A.; Diaz, R. Modelling greenhouse gas emissions for municipal solid waste management strategies in Ottawa, Ontario, Canada. *Resour. Conserv. Recycl.* **2008**, *52*, 1241–1251. [[CrossRef](#)]
7. Global Waste Management Outlook. 2016. Available online: <https://www.unenvironment.org/resources/report/global-waste-management-outlook> (accessed on 30 January 2020).
8. Fabry, F.; Rehmet, C.; Rohani, V.; Fulcheri, L. Waste gasification by thermal plasma: A review. *Waste Biomass Valorization* **2013**, *4*, 421–439. [[CrossRef](#)]
9. Arena, U.; Nelles, M.; Werther, J. Advanced aspects of thermal treatment of solid wastes: From a flue gas to a fuel gas technology? *Waste Manag.* **2012**, *32*, 623–624. [[CrossRef](#)] [[PubMed](#)]
10. Albores, P.; Petridis, K.; Dey, P.K. Analysing Efficiency of Waste to Energy Systems: Using Data Envelopment Analysis in Municipal Solid Waste Management. *Procedia Environ. Sci.* **2016**, *35*, 265–278. [[CrossRef](#)]
11. Rajasekhar, M.; Rao, N.V.; Rao, G.C.; Priyadarshini, G.; Kumar, N.J. Energy Generation from Municipal Solid Waste by Innovative Technologies – Plasma Gasification. *Procedia Mater. Sci.* **2015**, *10*, 513–518. [[CrossRef](#)]
12. Ruj, B.; Ghosh, S. Technological aspects for thermal plasma treatment of municipal solid waste-A review. *Fuel Process. Technol.* **2014**, *126*, 298–308. [[CrossRef](#)]
13. Gomez, E.; Rani, D.A.; Cheeseman, C.R.; Deegan, D.; Wise, M.; Boccaccini, A.R. Thermal plasma technology for the treatment of wastes: A critical review. *J. Hazard. Mater.* **2009**, *161*, 614–626. [[CrossRef](#)]
14. Samal, S. Thermal plasma technology: The prospective future in material processing. *J. Cleaner Prod.* **2017**, *142*, 3131–3150. [[CrossRef](#)]
15. Trelles, J.P.; Chazelas, C.; Vardelle, A.; Heberlein, J.V.R. Arc Plasma Torch Modeling. *J. Therm. Spray Technol.* **2009**, *18*, 728. [[CrossRef](#)]
16. Bai, L.; He, J.; Ouyang, Y.; Liu, W.; Liu, H.; Yao, H.; Li, Z.; Song, J.; Wang, Y.; Yuan, F. Modeling and selection of RF thermal plasma hot-wall torch for large-scale production of nanopowders. *Materials* **2019**, *12*, 2141. [[CrossRef](#)] [[PubMed](#)]
17. Rao, L.; Rivard, F.; Carabin, P. Thermal plasma torches for metallurgical applications. In Proceedings of the 4th International Symposium on High-Temperature Metallurgical Processing, San Antonio, TX, USA, 3–7 March 2013.
18. Ochoa Brezmes, A.; Breitkopf, C. Simulation of inductively coupled plasma with applied bias voltage using COMSOL. *Vacuum* **2014**, *109*, 52–60. [[CrossRef](#)]
19. Kim, T.H.; Kim, K.N.; Mishra, A.K.; Seo, J.S.; Jeong, H.B.; Bae, J.O.; Yeom, G.Y. Plasma characteristics of inductively coupled plasma using dual-frequency antennas. *Jpn. J. Appl. Phys.* **2013**, *52*, 5S2. [[CrossRef](#)]
20. Bernardi, D.; Colombo, V.; Coppa, G.G.M.; D’Angola, A. Simulation of the ignition transient in RF inductively-coupled plasma torches. *Eur. Phys. J. D.* **2001**, *14*, 337–348. [[CrossRef](#)]
21. Taghavipour, A.; Vajedi, M.; Azad, N.L. Nonlinear Model Predictive Control. In *Intelligent Control of Connected Plug-in Hybrid Electric Vehicles*; Advances in Industrial Control; Springer: Cham, Switzerland, 2019; pp. 45–47.
22. Wickramasinghe, D.G.C.; Narayana, M.; Witharana, S. Optimization of Process Parameters for Organic Municipal Solid Waste Torrefaction. In Proceedings of the 2019 Advances in Science and Engineering Technology International Conferences (ASET), Dubai, UAE, 26 March–10 April 2019.

